

A Journal of the Gesellschaft Deutscher Chemiker

Angewandte



International Edition

Chemie

[www.angewandte.org](http://www angewandte org)

Accepted Article

Title: Hydrazide Derivatives for Defect Passivation in Pure CsPbI₃ Perovskite Solar Cells

Authors: Yuhang Che, Zhike Liu, Yuwei Duan, Jungang Wang,
Shaomin Yang, Dongfang Xu, Wanchun Xiang, Tao Wang,
Ningyi Yuan, Jianning Ding, and Shengzhong (Frank) Liu

This manuscript has been accepted after peer review and appears as an Accepted Article online prior to editing, proofing, and formal publication of the final Version of Record (VoR). The VoR will be published online in Early View as soon as possible and may be different to this Accepted Article as a result of editing. Readers should obtain the VoR from the journal website shown below when it is published to ensure accuracy of information. The authors are responsible for the content of this Accepted Article.

To be cited as: *Angew. Chem. Int. Ed.* **2022**, e202205012

Link to VoR: <https://doi.org/10.1002/anie.202205012>

COMMUNICATION

WILEY-VCH

Hydrazide Derivatives for Defect Passivation in Pure CsPbI₃ Perovskite Solar Cells

Yuhang Che,^[a] Zhike Liu,^{*[a]} Yuwei Duan,^{*[a]} Jungang Wang,^[a] Shaomin Yang,^[a] Dongfang Xu,^[a] Wanchun Xiang,^[a] Tao Wang,^[a] Ningyi Yuan,^[c] Jianning Ding,^[c] and Shengzhong (Frank) Liu^{*[a,b]}

[a] Y. Che, Prof. Z. Liu, Dr. Y. Duan, J. Wang, S. Yang, D. Xu, Prof. W. Xiang, Prof. T. Wang, Prof. S. Liu
Key Laboratory of Applied Surface and Colloid Chemistry, Ministry of Education, Shaanxi Key Laboratory for Advanced Energy Devices, Shaanxi Engineering Lab for Advanced Energy Technology School of Materials Science and Engineering, Shaanxi Normal University, Xi'an, 710119 (China)
E-mail: zhike2015@snnu.edu.cn; yuwei-duan@snnu.edu.cn; szliu@dicp.ac.cn

[b] Prof. S. Liu
Dalian National Laboratory for Clean Energy iChEM, Dalian Institute of Chemical Physics Chinese Academy of Sciences, Dalian 116023 (China)
E-mail: szliu@dicp.ac.cn

[c] Prof. N. Yuan, Prof. J. Ding
Jiangsu Collaborative Innovation Center of Photovoltaic Science and Engineering, Jiangsu Province Cultivation Base for State Key Laboratory of Photovoltaic Science and Technology School of Materials Science and Engineering, Changzhou University, Changzhou 213164, China

Supporting information for this article is given via a link at the end of the document.

Abstract: All-inorganic CsPbI₃ perovskite presents preeminent chemical stability and desirable band gap as the front absorber for perovskite/silicon tandem solar cells. Unfortunately, CsPbI₃ perovskite solar cells (PSCs) still show low efficiency due to high density of defects in solution-prepared CsPbI₃ films. Herein, three kinds of hydrazide derivatives (benzoyl hydrazine (BH), formohydrazide (FH) and benzamide (BA)) are designed to reduce the defect density and stabilize the phase of CsPbI₃. Calculation and characterization results corroborate that the carboxyl and hydrazine groups in BH could form strong chemical bonds with Pb²⁺ ions, resulting in synergistic double coordination. In addition, the hydrazine group in BH also could form a hydrogen bond with iodine to assist the coordination. Consequently, a high efficiency of 20.47% is achieved, which is the highest PCE among all pure CsPbI₃-based PSCs reported to date. In addition, an unencapsulated device showed excellent stability in ambient air.

Introduction

Since a cesium lead iodide (CsPbI₃) perovskite solar cell (PSC) was first reported in 2015, CsPbI₃ perovskite has attracted great interest due to its excellent chemical stability and appropriate band gap (~1.7 eV) as the front sub-cell active layer for tandem solar cells.^[1-3] Regrettably, the highest power conversion efficiency (PCE) of CsPbI₃-based single junction PSCs still lags behind that of organic-inorganic hybrid PSCs with certified PCE over 25.7%, and even the CsPbI₃ PSCs with efficiency over 20% still suffer from a relatively high open-circuit voltage (V_{OC}) loss compared to organic-inorganic hybrid PSCs.^[4-8] Recent studies proposed that the major V_{OC} losses are correlated with the presence of deep defects in the CsPbI₃ active layer. This is attributed to the ionic nature of CsPbI₃ perovskite, which makes it prone to destruction under exposure to the external environment (moisture, light and heat) leading to the generation of a tremendous amount of nonradiative recombination centers.^[9-10] In addition, the low coordination among the Cs⁺ and [PbI₆]⁴⁻ octahedra leads to the phase instability of CsPbI₃ perovskite.^[11] Meanwhile, the defects (undercoordinated Pb²⁺, iodine vacancy, etc.) in CsPbI₃ can further weaken the interaction between Cs⁺ and [PbI₆]⁴⁻ octahedra to decrease the energy difference between the black and yellow phases.^[12] Therefore, it is important to decrease/passivate defects and solve the defect-triggered issues for highly efficient and stable CsPbI₃ PSCs.

In order to improve the photovoltaic performance and stability of inorganic PSCs, various passivation materials have been developed to eliminate/passivate the defects for reducing the nonradiative recombination losses in CsPbI₃ PSCs.^[13-19] Among them, the organic materials with C=O groups can passivate undercoordinated Pb²⁺ in perovskite film by Lewis base-acid reaction. For example, Huang's group introduced the ionic liquid solvent methylammonium acetate (MAAc) as an additive. The C=O group in MAAC has a strong interaction with PbI₂, and this interaction can retard the crystallization of the perovskite film and passivate Pb-related defects. The inorganic device with added MAAC exhibits an efficiency of 15.83% and V_{OC} of 1.32 V.^[20] Recently, Zhu's group explored a multifunctional additive 2-hydroxyethyl methacrylate (HEMA), and the C=O and C-OH in HEMA can interact with undercoordinated ions and provide coordination sites to passivate defects on the perovskite grain boundaries.^[21] Hydrazine derivatives with lone-pair electrons from the -NH₂ tail, including hydrazinium chloride (N₂H₅Cl), hydrazinium iodide (HAI), 4-hydrazinobenzoic acid (HBA), phenyl hydrazinium iodide (PHAI), carbohydrazide (CBH), etc., have also been explored as additives to passivate Pb-related

Accepted Manuscript

defects.^[22–25] For example, very recently, Huang's group utilized carbohydrazide (BH) as a solid-state lead-coordinating additive for organic-inorganic hybrid solar cells, delivering a maximum PCE of 23.6%.^[26] It is interesting to find that inserting carbonyl into hydrazine could decrease its reducibility and significantly enhance the coordination ability to bind with Pb^{2+} . Therefore, if hydrazine ligand ($-\text{NH}-\text{NH}_2$) is introduced at one end of a carbonyl group, the ability of the resulting $-\text{C}=\text{O}-\text{NH}-\text{NH}_2$ material to passivate Pb-related defects will be greatly enhanced by using the synergistic coordination effect of the $\text{C}=\text{O}$ and $-\text{NH}-\text{NH}_2$ ligand. The hydrazide group also can form a hydrogen bond with iodine to assist the $\text{C}=\text{O}$ binding with Pb-related defects and maximize passivator-defect binding. At the same time, if an electron conjugative unit is introduced at the other end of $-\text{C}=\text{O}-\text{NH}-\text{NH}_2$ material, the coordination between the new material and Pb^{2+} will be further improved, which is conducive to the preparation of highly effective passivation materials.

In this work, three kinds of hydrazide derivatives (BH, FH and BA) were selected to systematically study the synergistic passivation effect of carbonyl, hydrazine and phenyl groups on perovskite defects. Theoretical calculation and comprehensive characterizations corroborated that the carboxyl and hydrazine groups in BH could be tightly adsorbed on Pb^{2+} by synergistic double coordination to passivate shallow- and deep-level defects, i.e., by increasing the energy barrier for lattice distortion, and phenyl in the BH could strength such coordination through its electron conjugative properties. Furthermore, the addition of BH leads to optimized energy-level alignment to facilitate charge transfer between the perovskite and hole transport material. Benefiting from the above effects, the champion device with BH additive delivers an excellent PCE of 20.47% with ultrahigh V_{OC} of 1.24 V, which is the highest reported PCE for pure CsPbI_3 PSCs to date (Table S1). In addition, the BH- CsPbI_3 based unencapsulated device maintains more than 98% of their initial efficiency after 1000 h of storage in ambient air.

Results and Discussion

Electrostatic potential (ESP) analysis was conducted to elaborate the structure-property relationships of BH, FH and BA, as in Figure 1a. Compared with FH, the electron cloud density of $\text{C}=\text{O}$ in BH and BA is lower because the phenyl delocalizes the π electron from $\text{C}=\text{O}$. The phenyl can also decrease the electron cloud density of nitrogen close to $\text{C}=\text{O}$ to weaken the reducibility and enhance the stability of BH. The electron cloudy density of the nitrogen from the tail NH_2 in BH is almost the same as that of FH, suggesting that the phenyl in BH has less influence on the tail NH_2 . Density functional theory (DFT) was adopted to simulate the chemical interaction models and calculate the defect-binding energies of BH-Pb^{2+} , FH-Pb^{2+} and BA-Pb^{2+} .^[27] Figure 1b exhibits the optimized configuration of the BH, FH and BA molecules on the surface of CsPbI_3 and the corresponding Pb^{2+} vacancy defects. All the molecules with $\text{C}=\text{O}$ and NH_2 groups could form double coordination bonds with Pb^{2+} , a pentatomic ring was formed when BH/FH binded with Pb^{2+} while a tetratomic ring was formed for BA- Pb^{2+} . It is well-known that the pentatomic ring is much more stable than the tetratomic ring, which indicates that BH/FH with the hydrazide group can passivate Pb^{2+} -related defects more effectively than BA with the amide group. The binding energies of E_{NH_2} ($\text{NH}_2-\text{Pb}^{2+}$), $E_{\text{C}=\text{O}}$ ($\text{C}=\text{O}-\text{Pb}^{2+}$) and $E_{(\text{C}=\text{O} + \text{NH}_2)}$ ($(\text{C}=\text{O} + \text{NH}_2)-\text{Pb}^{2+}$) for BH, FH and BA are summarized in Figure 1c. The values of $E_{(\text{C}=\text{O} + \text{NH}_2)}$ (-2.14 eV for BH, -1.87 eV for FH, -1.26 eV for BA) are higher than those of E_{NH_2} or $E_{\text{C}=\text{O}}$ for BH-, FH- and BA- Pb^{2+} , which means that all the BH, FH and BA molecules prefer to bind Pb^{2+} with $\text{C}=\text{O}$ and NH_2 in combination rather than alone. Therefore, compared with BA and FH, the BH has the highest value of $E_{(\text{C}=\text{O} + \text{NH}_2)}$ (-2.14 eV), indicating that BH could passivate Pb^{2+} -related defects more effectively than FH and BA to reduce the defect density. As confirmed by Figure 1d and Fig. S1, the formation energy of the Pb vacancy defect (V_{Pb}) in BH- CsPbI_3 (-2.96 eV) is significantly higher than those of the control (-0.96 eV), FH- CsPbI_3 (-2.35 eV) and BA- CsPbI_3 (-1.87 eV).

Then, the influence of BH, FH, and BA additives on perovskite films was studied experimentally. To evaluate the influence on the lattice structure of the CsPbI_3 film, the crystallinities of perovskite films were analyzed by X-ray diffraction (XRD) (Figure 2a, Fig. S2a). Both the control CsPbI_3 film and target CsPbI_3 films with 3% BH, FH and BA additives (BH- CsPbI_3 , FH- CsPbI_3 and BA- CsPbI_3) showed a well-crystallized γ -phase CsPbI_3 .^[28] The intensities of the (110) and (220) peaks for BH- CsPbI_3 film are higher than those of FH- CsPbI_3 and BA- CsPbI_3 films, indicating that BH can facilitate the preferred <110>-oriented growth of the γ - CsPbI_3 .^[29] The UV-Vis absorption spectra of CsPbI_3 films are shown in Figure 2b and Fig. S2b. All the CsPbI_3 films show very similar absorption ranges, indicating that the additives do not alter the band gap ($E_g = 1.71$ eV) of the CsPbI_3 films.^[30] The BH- CsPbI_3 film shows an improved absorption intensity in the range from 500 to 850 nm.

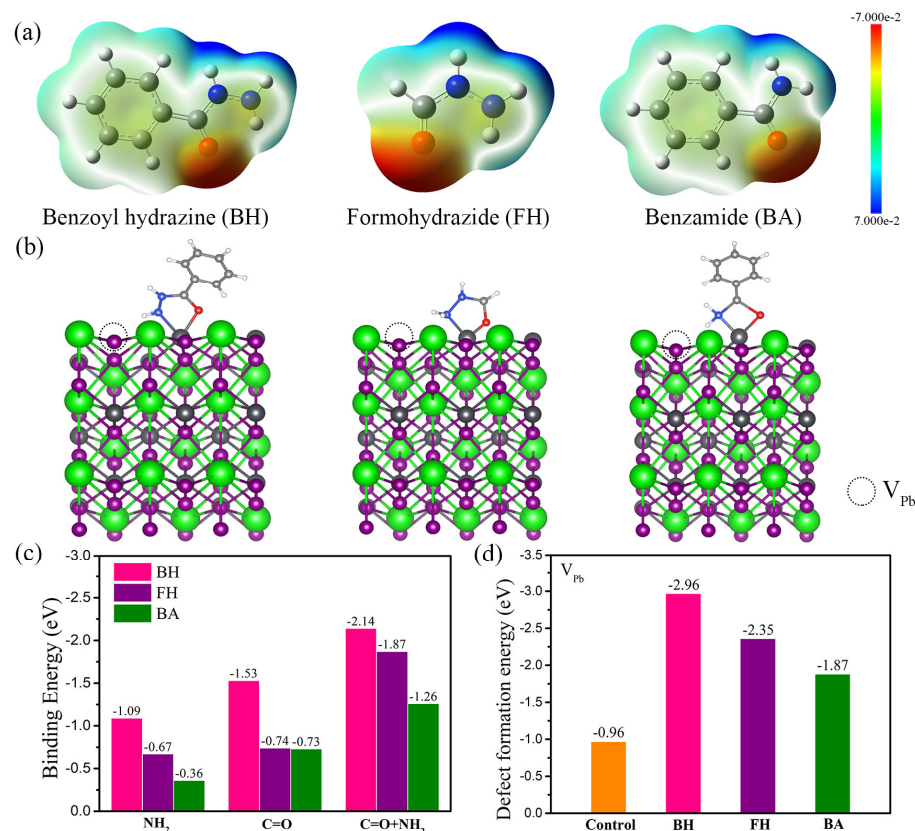


Figure 1. a) The electrostatic potential (ESP) analysis of BH, FH, and BA. b) The Pb^{2+} vacancy defect and the models and sites for interaction between undercoordinated Pb^{2+} and BH, FH, and BA via C=O and NH₂ groups, respectively. c) The binding energies of NH₂- Pb^{2+} , C=O- Pb^{2+} and (C=O + NH₂)- Pb^{2+} for BH, FH and BA, respectively. d) The formation energies of the Pb^{2+} vacancy defect in CsPbI₃ treated by BH, FH and BA, respectively.

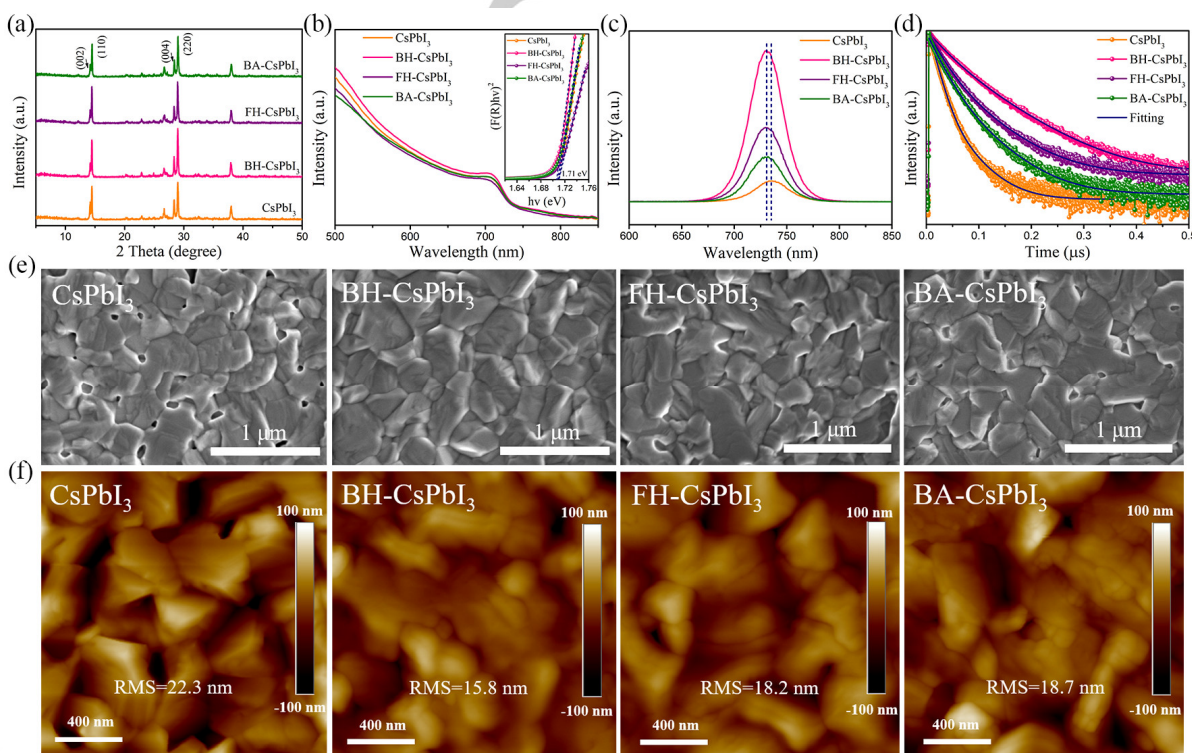


Figure 2. a) The XRD patterns, b) UV-Vis curves, c) steady-state PL curves, d) TRPL spectra, e) SEM images and f) AFM images for control CsPbI₃ film, and CsPbI₃ films treated by BH, FH and BA, respectively.

Steady-state photoluminescence (PL) and time-resolved photoluminescence (TRPL) characteristics were utilized to explore the charge recombination and transport process in these CsPbI_3 films (Figure 2c, Fig. S3).^[31-32] The BH-CsPbI₃ film exhibits the strongest fluorescent intensity (6.6-fold that of the control film) among all the perovskite films, indicating the lowest non-radiative recombination, which could be ascribed to the more effective passivation of defects by BH. Meanwhile, the PL peaks of all the perovskite films with additives are blue-shifted from 734 nm for the control to 730 nm, indicating the trap defects in the band gap were significantly passivated. The TRPL spectra are shown in Figure 2d, and the fitted parameters are summarized in Tables S2 and S3. The average lifetime (τ_{ave}) of excited electrons was prolonged from 19.32 ns (CsPbI_3) to 66.28 ns (BH-CsPbI₃), which is much longer than 44.65 ns for FH-CsPbI₃ and 36.37 ns for BA-CsPbI₃. Therefore, the non-radiative recombination in the perovskite layer was significantly suppressed by BH. Femtosecond transient absorption (fs-TA) spectra were obtained to further study the influence of BH, FH and BA additives on the carrier lifetimes of CsPbI_3 films (Fig. S4).^[33] The carrier decay dynamic curves illustrate that the BH-CsPbI₃ film has a longer lifetime than the others. The PL, TRPL and fs-TA results corroborate that the BH can effectively passivate the CsPbI_3 film and enhance its electrical properties.

To evaluate the influence of additives on the morphology of perovskite films, top-view scanning electron microscopy (SEM) and atomic force microscopy (AFM) were conducted (Figure 2e, 2f, S5-7). The CsPbI_3 film exhibits many pinholes on the surface, which will lead to surface recombination and affect charge transfer and collection. For the BH-, FH- and BA-CsPbI₃ films, the density of surface pinholes shows a decreasing trend, and the surface pinholes of BH-CsPbI₃ film have almost disappeared. The AFM results show that BH-CsPbI₃ film exhibits the smallest root-mean-square roughness and minimum pinhole density among all the CsPbI_3 films, which is consistent with the SEM results.

X-ray photoelectron spectroscopy (XPS) was conducted to confirm the interaction between the perovskite and BH, FH and BA (Figure 3).^[34] As shown in Figure 3a, both the Pb^{2+} 4f (143.21 eV for $4f_{7/2}$ and 138.35 eV for $4f_{5/2}$) and I⁻ 3d (630.21 eV for $3d_{5/2}$ and 618.72 eV for $3d_{3/2}$) peaks displayed the largest shifts for BH-CsPbI₃ film (0.27 eV for Pb^{2+} and 0.21 eV for I⁻) toward higher binding energy among the BH-, FH- and BA-CsPbI₃ films, indicating the strongest interaction between the BH and PbI_2 , which originates from the synergistic double coordination interaction (C=O-Pb^{2+} and $-\text{NH-NH}_2\text{-Pb}^{2+}$) and the hydrogen bond ($\text{NH}_2^-\cdots\text{I}^-$) formation.^[35] The signals of metallic Pb at 141.32 and 136.46 eV were reduced more distinctly in BH-CsPbI₃ film than in BA-CsPbI₃ film, but slightly enhanced in FH-CsPbI₃ film, which is due to the higher reducibility for FH additive.^[36] Compared with BH and FH, the smaller shift of O 1s for BA (0.05 eV) further illustrates the weaker interaction between the C=O in BA and Pb^{2+} . Furthermore, it is obvious that the movement of N 1s for BH (0.96 eV) and FH (0.76 eV) are more than 3-fold larger than for BA (0.21 eV), which indicates that the $-\text{NH-NH}_2$ in BH/FH can strengthen the interaction between BH/FH and CsPbI₃ film through forming a coordinate bond with Pb^{2+} and hydrogen bond with I⁻, which is consistent with the results obtained from DFT calculation (Figure 1c). Therefore, these XPS results suggest that C=O and $-\text{NH-NH}_2$ groups can form strong interactions with perovskite through synergistic double-coordination and hydrogen bonds, and the phenyl group not only strengthens the bonds with perovskite but also suppresses the formation of metallic Pb due to its electron conjugative effect.

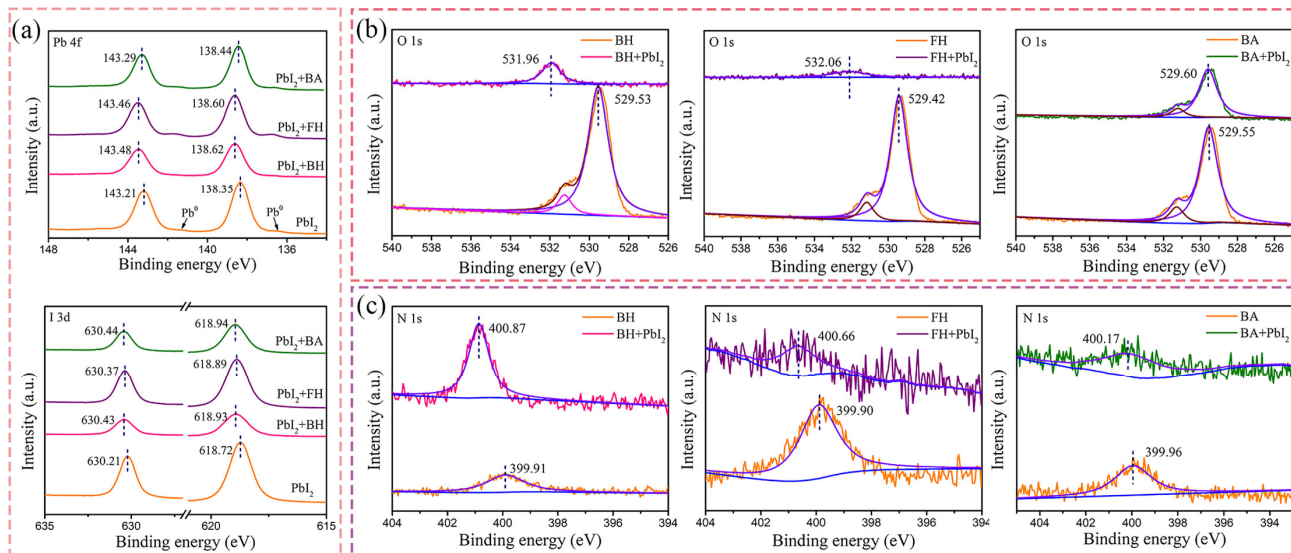


Figure 3. The XPS a) Pb 4f and I 3d, b) O 1s and c) N 1s spectra for PbI_2 , BH, FH, BA, PbI_2+BH , PbI_2+FH , and PbI_2+BA , respectively.

Liquid-state ^1H nuclear magnetic resonance ($^1\text{H-NMR}$) was employed to further elucidate the interaction between the additives (BH, FH, BA) and PbI_2 (Fig. S8). The proton resonance signals for -NH- and -NH₂ in BH shifted from 9.91 to 10.27 ppm (~ 0.36 ppm) and from 4.64 to 5.02 ppm (~ 0.38 ppm), respectively, and broadened after the addition of PbI_2 (Figure 4a). Those downfield shifts could be ascribed to the formation of -NH-NH₂-Pb²⁺ ligands, which was further confirmed by Mass Spectrum (MS) (Fig. S9). A new compound $[\text{C}_7\text{H}_8\text{N}_2\text{OPb}]^{2+}$ with molecular weight (MW) of 343.990 was produced. By removing the phenyl group from BH for FH (Figure 4b), although similar downfield shifts and broadening trends of -NH- and -NH₂ were observed in FH after addition of PbI_2 , the shifts of -NH- (0.33 ppm) and -NH₂ (0.26 ppm) are smaller than those for BH, indicating a weaker interaction between FH and Pb²⁺ with respect to BH. The MS also confirms a new compound $[\text{CH}_4\text{N}_2\text{OPb}]^{2+}$ with MW of 268.322 was produced (Fig. S10). When the BH was tailored to remove the -NH₂ tail for BA (Figure 4c), a much small shift (0.04 ppm) and broadening for -NH₂ in BA was observed after addition of PbI_2 , suggesting a very weak interaction between BA and PbI_2 , which was also confirmed by MS. An extremely weak compound peak for $[\text{C}_7\text{H}_7\text{NOPb}]^{2+}$ with MW of 329.049 is observed (Fig. S11).

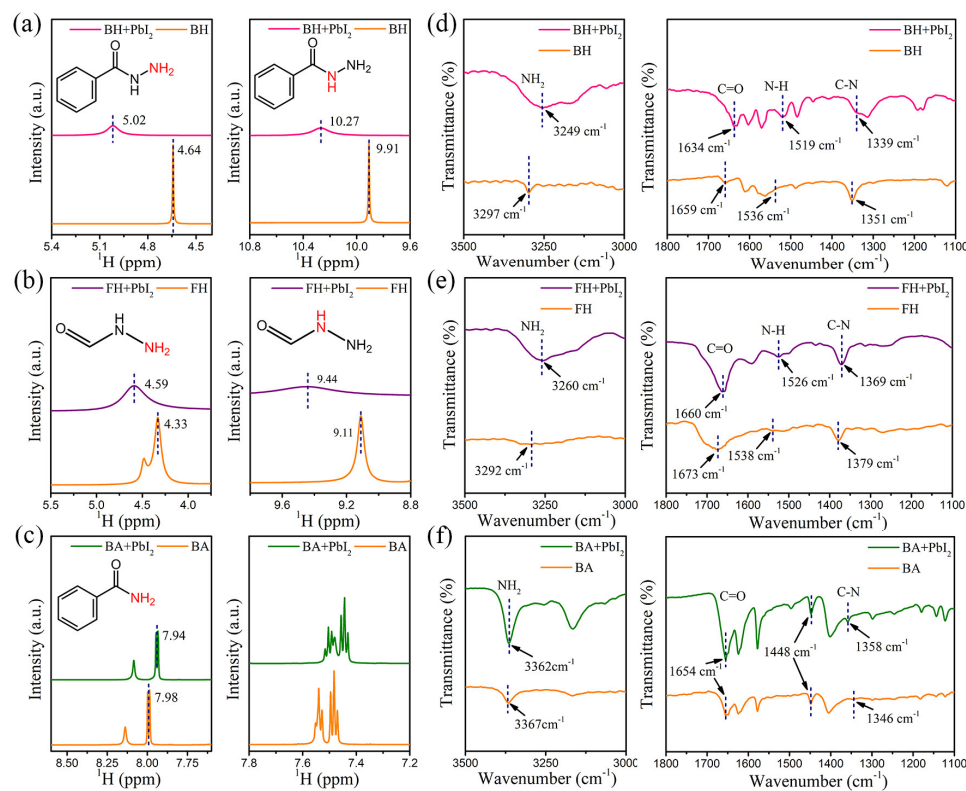


Figure 4. The ^1H NMR spectra of a) BH and BH + PbI₂, b) FH and FH + PbI₂, and c) BA and BA + PbI₂, respectively. The FTIR spectra of d) BH and BH + PbI₂, e) FH and FH + PbI₂, and f) BA and BA + PbI₂, respectively.

Fourier-transform infrared (FTIR) spectra were adopted to further illustrate the interaction between the additives (BH, FH, BA) and PbI_2 (Fig. S12). As shown in Figure 4d and Table S4, the absorption peaks of N-H asymmetric stretching ($\nu_{\text{N-H}}$), N-H bending ($\delta_{\text{N-H}}$), C=O stretching ($\nu_{\text{C=O}}$) and C-N stretching ($\nu_{\text{C-N}}$) in BH were clearly observed at wavenumbers of 3297, 1536, 1659, and 1351 cm⁻¹, respectively. By introducing PbI_2 into the BH film, several changes can be found in the FTIR spectra. First, the $\nu_{\text{N-H}}$ peak at 3297 cm⁻¹ shifted to 3249 cm⁻¹ and broadened. Second, the $\delta_{\text{N-H}}$ peak at 1536 moved to 1519 cm⁻¹ accompanied with the downshifts of $\nu_{\text{C=O}}$ from 1659 to 1634 cm⁻¹ and $\nu_{\text{C-N}}$ from 1351 to 1339 cm⁻¹. It is reasonable to deduce that those distinct downshifts stem from the interaction between BH and PbI_2 because PbI_2 has no FTIR peaks in those ranges. By removing phenyl from BH for FH, a similar downshift tendency was observed in the FH and PbI_2 film compared with pure FH (Figure 4e). However, the downshifts are smaller than those for the BH + PbI₂ film, further indicating that the phenyl can strengthen the interaction between BH and PbI_2 by the formation of strong conjugation between the benzene ring and C=O. When the BH was tailored to remove -NH tail for BA (Figure 4f), the shifts of $\nu_{\text{N-H}}$ and $\nu_{\text{C=O}}$ from BA to BA + PbI₂ film are negligible compared with those in the BH + PbI₂ or FH + PbI₂ films, further suggesting that the -NH-NH₂ group can not only form a strong interaction with Pb²⁺ but also enhance the interaction between C=O and Pb²⁺. The above XPS, NMR and FTIR results systematically proved that BH with both phenyl and hydrazide groups can combine with perovskite better than FH or BA to achieve effective passivation.

In order to examine the effect of additives on photovoltaic performance, PSCs were fabricated with the FTO/TiO₂/CsPbI₃ (BH/FH/BA)/Spiro-OMeTAD/Au structure, as shown in Figure 5a. Cross-sectional SEM images of the CsPbI₃ devices without and with additives are shown in Fig. S13. Ultraviolet photoelectron spectroscopy (UPS) was implemented to explore the impact of the additives on the conduction band (CB), valence band (VB) and Fermi energy (E_F) of the perovskite films, and the detailed parameters are shown in Fig. S14 and Table S5. The VB values are extracted as -5.69, -5.47, -5.54 and -5.58 eV for control CsPbI₃ and BH-CsPbI₃, FH-CsPbI₃ and BA-CsPbI₃ perovskite films, respectively. By subtracting the band gap (1.71 eV obtained from UV-Vis) from the corresponding VB, the values of the CB are estimated to be -3.98, -3.76, -3.83 and -3.87 eV, respectively. The energy-level alignments of control CsPbI₃, BH-CsPbI₃, FH-CsPbI₃ and BA-CsPbI₃ layers in PSCs are depicted in Figure 5b. The Fermi levels of BA-CsPbI₃, FH-CsPbI₃ and BH-CsPbI₃ films are in an ascending order, which are consistent with trend of their passivation abilities.^[37] The n-type BH-CsPbI₃ film exhibits the highest VB and Fermi level, which is conducive to hole transfer from the perovskite to Spiro-OMeTAD and the construction of a high built-in potential with p-type Spiro-OMeTAD.^[38]

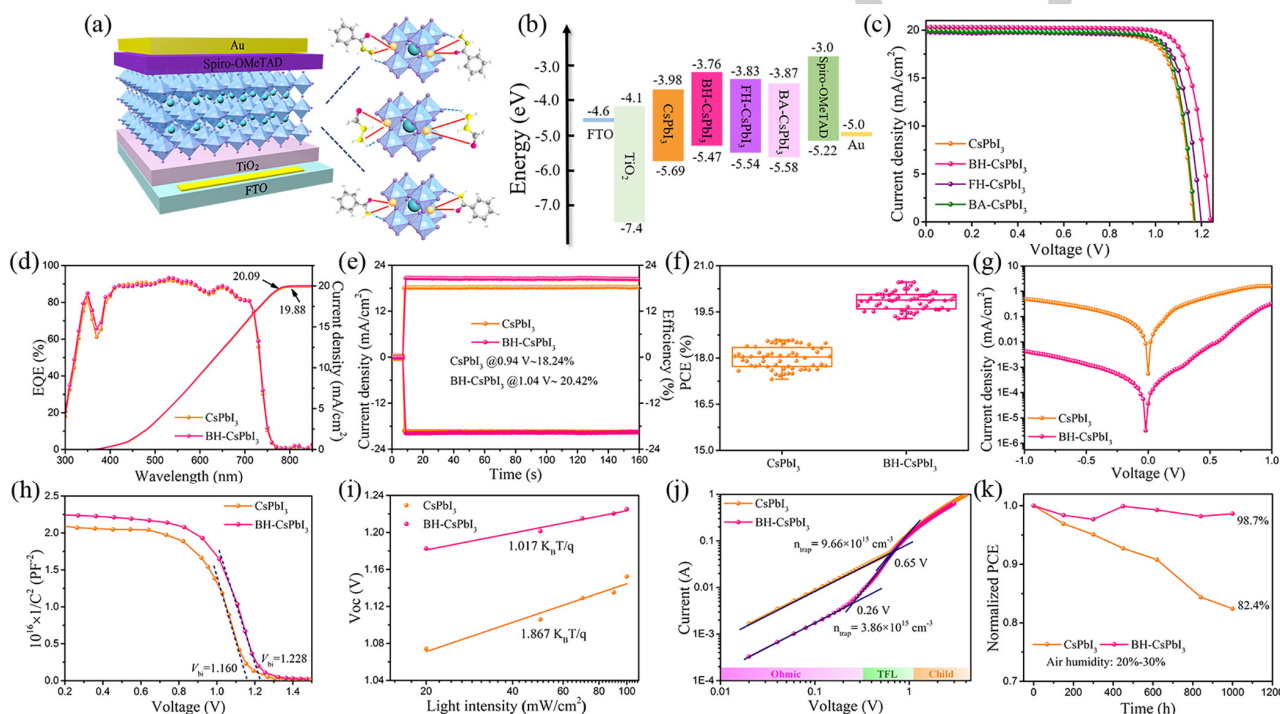


Figure 5. a) The device architecture and presumed interaction models of BH, FH and BA towards perovskite films, b) The schematic energy-level alignment of CsPbI₃, BH-CsPbI₃, FH-CsPbI₃ and BA-CsPbI₃ films, c) The J-V curves of CsPbI₃ and BH-CsPbI₃, FH-CsPbI₃ and BA-CsPbI₃ devices, d) The EQE spectrum and integrated current density, e) the stable output curves, f) PCE statistics of 40 CsPbI₃ and 40 BH-CsPbI₃ devices, g) dark J-V curves of CsPbI₃ and BH-CsPbI₃ devices, h) Mott-Schottky curves, i) V_{oc} versus light intensity plots, j) space-charge-limited current versus voltage curves of electron-only devices and k) the air stability of CsPbI₃ and BH-CsPbI₃ PSCs.

Table 1 The summary of the photovoltaic parameters for CsPbI₃, BH-CsPbI₃, FH-CsPbI₃ and BA-CsPbI₃ PSCs, respectively.

Samples	Voc (V)	Jsc (mA/cm ²)	FF (%)	PCE (%)
CsPbI ₃	1.166	19.92	79.92	18.57
BH-CsPbI ₃	1.241	20.30	81.23	20.47
FH-CsPbI ₃	1.199	19.78	81.10	19.24
BA-CsPbI ₃	1.172	19.94	81.53	19.05

The J-V curves of CsPbI₃ without and with additives are shown in Figure 5c, and the corresponding photovoltaic parameters are listed in Table 1. The concentrations of additives were optimized, and the corresponded photovoltaic results are summarized in Fig. S15-S17 and Table S6-S8. The CsPbI₃ device delivers a PCE of 18.57% with V_{oc} of 1.166 V, J_{sc} of 19.92 mA cm⁻² and FF of 79.92%. The BH-CsPbI₃ device yields a champion PCE of 20.47% with V_{oc} of 1.241 V, J_{sc} of 20.30 mA cm⁻² and FF of 81.23%. The improved

V_{OC} can be ascribed to the evaluated CB and the enhanced built-in potential (V_{bi}) in the perovskite film as described above. The validity of J_{SC} was checked by external quantum efficiency (EQE) measurements (Figure 5d). The corresponding integrated currents for the control and BH-CsPbI₃ devices are 20.09 and 19.88 mA cm⁻², respectively, which agree well with the J-V results. In addition, the BH-CsPbI₃ device gives a steady-state PCE output of 20.42% under a constant bias voltage of 1.04 V, while the CsPbI₃ device only delivers a steady-state PCE of 18.24%, as depicted in Figure 5e. The statistical distributions of photovoltaic parameters for 40 CsPbI₃ devices and 40 BH-CsPbI₃ devices are summarized in Figure 5f and Fig. S18. The BH-CsPbI₃ devices exhibit good repeatability with the lower fluctuation of PCE compared with the CsPbI₃ devices. As shown in Figure 5g, The BH-CsPbI₃ device shows much lower leakage current than the CsPbI₃ device, indicating a decreased carrier generation rate, which is related to the trap density in the device.^[39]

To further elucidate the higher V_{OC} obtained from BH-CsPbI₃ devices, capacitance-voltage (C-V) test was implemented to determine the built-in potential (V_{bi}) following the Mott-Schottky method (Figure 5h).^[40] The V_{bi} can be obtained from the intercept of the linear regime with the x-axis of the Mott-Schottky plot. It is obvious that the V_{bi} of 1.228 V for BH-CsPbI₃ device is larger than the 1.160 V for the CsPbI₃ device. The V_{bi} value is well-matched with the V_{OC} corresponding to the BH-CsPbI₃ device. The larger V_{bi} value can provide more efficient charge separation and collection, which is favorable for achieving higher V_{OC} . To clarify the improved FF, we studied the charge carrier recombination in the PSCs. The V_{OC} as a function of incident light intensity was measured (Figure 5i).^[41] The ideality factor ($n = 1.017 \text{ kT/q}$) for the BH-CsPbI₃ device is closer to 1 kT/q and much smaller than that of the CsPbI₃ device ($n = 1.867 \text{ kT/q}$), which manifests that bimolecular recombination is dominant in the BH-CsPbI₃ PSCs and the trap-assisted recombination was significantly inhibited by adding BH. To quantitatively evaluate the impact of BH additive on the defect density of the perovskite film, electron-dominated devices with the structure FTO/TiO₂/CsPbI₃(BH)/PCBM/Ag were fabricated and tested via the space charge-limited current (SCLC) method under dark conditions (Figure 5j). The trap density is calculated from the trap-filling limit voltage (V_{TFL}) through the SCLC model.^[42] As expected, the BH-CsPbI₃ device holds the lower value of V_{TFL} (0.26 V) with the n_{trap} of $3.86 \times 10^{15} \text{ cm}^{-3}$, which is much lower than that of the CsPbI₃ device ($V_{TFL} = 0.65 \text{ V}$; $n_{trap} = 9.66 \times 10^{15} \text{ cm}^{-3}$), confirming that BH additive can greatly suppress the defects of perovskite film. In addition, the electrochemical impedance spectra (EIS) were measured under dark conditions to further assess the charge transport and recombination properties of devices (Fig. S19, Table S9). The BH-CsPbI₃ device holds the smaller series resistance ($R_s = 22.03 \Omega$) and larger recombination resistance ($R_{rec} = 6467 \Omega$) compared with the CsPbI₃ device ($R_s = 30.51 \Omega$, $R_{rec} = 2436 \Omega$), respectively, which means that the charge extraction and transport in the BH-CsPbI₃ device are more efficient. The device stability was tested without any encapsulation in ambient conditions (temperature: 25 °C, relative humidity: 20~30%). As shown in Figure 5k, the BH-CsPbI₃ device maintained 98.7% of its initial PCE after storing 1000 h in air and is much more stable than the CsPbI₃ device (82.4%).

Conclusion

In this work, through the regulation of molecular structure, an effective multifunctional passivator was selected on the basis of calculation and experiments. The new passivator (BH) with carboxyl, hydrazine and phenyl groups can form strong interaction with undercoordinated Pb²⁺ and I⁻ through synergistic interaction to minimize the trap density and prolong the carrier lifetime, which is corroborated by comprehensive characterization. Consequently, the BH-CsPbI₃ device displays an excellent efficiency of 20.47%, which is the highest value for pure CsPbI₃ PSC, with robust stability in ambient atmosphere for 1000 h. This work provides positive and constructive information to expedite design strategies for new passivators.

Acknowledgements

The authors acknowledge support from the National Natural Science Foundation of China (62074095), the Fundamental Research Funds for the Central Universities (GK202002001), the 111 Project (Grant No. B21005), and the DNL Cooperation Fund CAS (DNL180311).

Conflict of interest

The authors declare no conflict of interest.

Additional information**Supplemental Information**

Supplemental Information includes nineteen Figures and nine Tables.

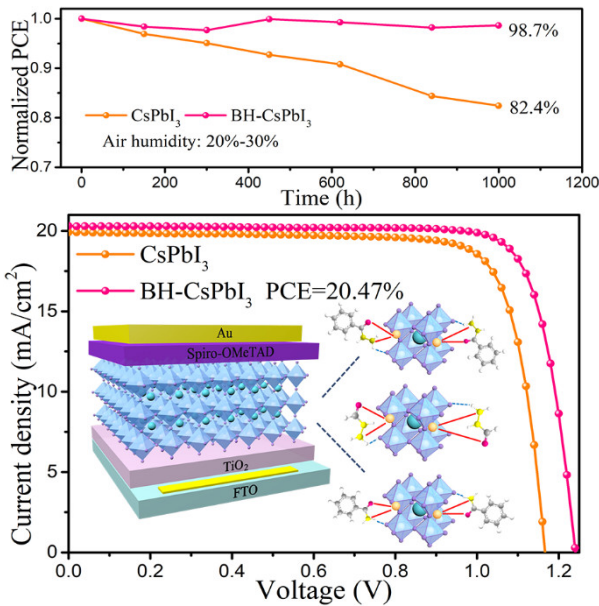
Keywords: CsPbI₃ • defect passivation • hydrazide • perovskite • solar cells**References**

- [1] F. Fabregat-Santiago, J. Bisquert, L. Cevey, P. Chen, M. K. Wang, S. M. Zakeeruddin, M. Grätzel, *J. Am. Chem. Soc.*, **2009**, *131*, 558-562.
- [2] G. E. Eperon, G. M. Paterno, R. J. Sutton, A. Zampetti, A. A. Haghhighirad, F. Cacialli, H. J. Snaith, *J. Mater. Chem. A*, **2015**, *3*, 19688-19695.
- [3] Y. Wang, T. Y. Zhang, M. Kan, Y. X. Zhao, *J. Am. Chem. Soc.*, **2018**, *140*, 12345-12348.
- [4] T. H. Wu, Z. Z. Qin, Y. B. Wang, Y. Z. Wu, W. Chen, S. F. Zhang, M. L. Cai, S. Y. Dai, J. Zhang, J. Liu, Z. M. Zhou, X. Liu, H. Segawa, H. R. Tan, Q. W. Tang, J. F. Fang, Y. W. Li, L. M. Ding, Z. J. Ning, Y. B. Qi, Y. Q. Zhang, L. Y. Han, *Nano-Micro Lett.*, **2021**, *13*, 152.
- [5] W. C. Xiang, S. Z. Liu, W. Tress, *Energy Environ. Sci.*, **2021**, *14*, 2090-2113.
- [6] H. Min, D. Y. Lee, J. Kim, G. Kim, K. S. Lee, J. Kim, M. J. Paik, Y. K. Kim, K. S. Kim, M. G. Kim, T. J. Shin, S. I. Seok, *Nature*, **2021**, *598*, 444-450.
- [7] Y. Wang, M. I. Dar, L. K. Ono, T. Y. Zhang, M. Kan, Y. W. Li, L. J. Zhang, X. T. Wang, Y. G. Yang, X. Y. Gao, Y. B. Qi, M. Grätzel, Y. X. Zhao, *Science*, **2019**, *365*, 591-595.
- [8] Z. Y. Ni, C. X. Bao, Y. Liu, Q. Jiang, W. Q. Wu, S. S. Chen, X. Z. Dai, B. Chen, B. Hartweg, Z. S. Yu, Z. Holman, J. S. Huang, *Science*, **2020**, *367*, 1352-1358.
- [9] Y. Wei, Z. Y. Cheng, J. Lin, *Chem. Soc. Rev.*, **2019**, *48*, 310-350
- [10] Y. Y. Zhou, Y. X. Zhao, *Energy Environ. Sci.*, **2019**, *12*, 1495-1511.
- [11] D. B. Straus, S. Guo, R. J. Cava, *J. Am. Chem. Soc.*, **2019**, *141*, 11435-11439.
- [12] Y. H. Kye, C. J. Yu, U. G. Jong, K. C. Ri, J. S. Kim, S. H. Choe, S. N. Hong, S. Z. Li, J. N. Wilson, A. Walsh, *J. Phys. Chem. C*, **2019**, *123*, 9735-9744.
- [13] H. L. Wang, Z. J. Dong, H. C. Liu, W. P. Li, L. Q. Zhu, H. N. Chen, *Adv. Energy Mater.*, **2021**, *11*, 2002940.
- [14] Y. Wang, Y. T. Chen, T. Y. Zhang, X. T. Wang, Y. X. Zhao, *Adv. Mater.*, **2020**, *32*, 2001025.
- [15] Y. T. Chen, X. M. Liu, Y. X. Zhao, *Angew. Chem. Int. Ed.*, **2021**, *61*, e202110603.
- [16] J. R. Zhang, G. Hodes, Z. W. Jin, S. Z. Liu, *Angew. Chem. Int. Ed.*, **2019**, *58*, 15596-15618.
- [17] Q. F. Ye, F. Ma, Y. Zhao, S. Q. Yu, Z. M. Chu, P. Q. Gao, X. W. Zhang, J. B. You, *Small*, **2020**, *16*, 2005246.
- [18] F. Ke, C. X. Wang, C. J. Jia, N. R. Wolf, J. J. Yan, S. Y. Niu, T. P. Devereaux, H. I. Karunadasa, W. L. Mao, Y. Lin, *Nature Commun.*, **2021**, *12*, 461-468.
- [19] J. W. Hou, P. Chen, A. Shukla, A. Krajnc, T. S. Wang, X. M. Li, R. Doasa, Luiz H. G. Tizei, B. Chan, D. N. Johnstone, R. J. Lin, T. U. Schülli, I. Marten, D. Appadoo, M. S' Ari, Z. L. Wang, T. Wei, S. -C. Lo, M. Y. Lu, S. C. Li, E. B. Namdas, G. Mali, A. K. Cheetham, S. M. Collins, V. Chen, L. Z. Wang, T. D. Bennett, *Science*, **2021**, *374*, 621-625.
- [20] X. J. Wang, X. Q. Ran, X. T. Liu, H. Gu, S. W. Zuo, W. Hui, H. Lu, B. Sun, X. Y. Gao, J. Zhang, Y. D. Xia, Y. H. Chen, W. Huang, *Angew. Chem. Int. Ed.*, **2020**, *59*, 13354-13361.
- [21] S. Q. Fu, J. B. Wang, X. H. Liu, H. B. Yuan, Z. X. Xu, Y. J. Long, J. Zhang, L. K. Huang, Z. Y. Hu, Y. J. Zhu, *Chem. Eng. J.*, **2021**, *422*, 130572.
- [22] M. E. Kayesh, T. H. Chowdhury, K. Matsuishi, R. Kaneko, S. Kazaoui, J.-J. Lee, T. Noda, A. Islam, *ACS Energy Lett.*, **2018**, *3*, 1584-1589.
- [23] F. Z. Li, C. S. Zhang, J. H. Huang, H. C. Fan, H. J. Wang, P. C. Wang, C. L. Zhan, C. M. Liu, X. J. Li, L. M. Yang, Y. L. Song, K. J. Jiang, *Angew. Chem. Int. Ed.*, **2019**, *58*, 6688-6692.
- [24] M. A. Rahman Laskar, W. Q. Luo, N. Ghimire, A. H. Chowdhury, B. Bahrami, A. Gurung, K. M. Reza, R. Pathak, R. S. Bobba, B. S. Lamsal, K. Chen, M. T. Rahman, S. I. Rahman, K. Emshadi, T. T. Xu, M. Liang, W.-H. Zhang, Q. Q. Qiao, *Adv. Funct. Mater.*, **2020**, *30*, 2000778.
- [25] J. P. Cao, H.-L. Loi, Y. Xu, X. Y. Guo, N. X. Wang, C.-K. Liu, T. Y. Wang, H. Y. Cheng, Y. Zhu, M. G. Li, W.-Y. Wong, F. Yan, *Adv. Mater.*, **2022**, *34*, 2107729.
- [26] S. S. Chen, X. Z. Dai, S. Xu, H. Y. Jiao, L. Zhao, J. S. Huang, *Science*, **2021**, *373*, 902-907.
- [27] X. J. Gu, W. C. Xiang, Q. W. Tian, S. Z. Liu, *Angew. Chem. Int. Ed.*, **2021**, *60*, 23164-23170.
- [28] B. Y. Zhao, S. F. Jin, S. Huang, N. Liu, J.-Y. Ma, D.-J. Xue, Q. W. Han, J. Ding, Q.-Q. Ge, Y. Q. Feng, J.-S. Hu, *J. Am. Chem. Soc.*, **2018**, *140*, 11716-11725.
- [29] A. Marronnier, G. Roma, S. B. Richard, L. Pedesseau, J.-M. Jancu, Y. Bonnassieux, C. Katan, C. C. Stoumpos, M. G. Kanatzidis, J. Even, *ACS Nano*, **2018**, *12*, 3477-3486.
- [30] S. M. Yoon, H. Min, J. B. Kim, G. Kim, K. S. Lee, S. I. Seok, *Joule*, **2021**, *5*, 183-196.
- [31] Y. Han, H. Zhao, C. Y. Duan, S. M. Yang, Z. Yang, Z. K. Liu, S. Z. Liu, *Adv. Funct. Mater.*, **2020**, *30*, 1909972.
- [32] S. M. Yang, J. L. Wen, Z. K. Liu, Y. H. Che, J. Xu, J. G. Wang, D. F. Xu, N. Y. Yuan, J. N. Ding, Y. W. Duan, S. Z. Liu, *Adv. Energy Mater.*, **2021**, *2103019*.
- [33] Q. Cao, J. B. Yang, T. Wang, Y. K. Li, X. Y. Pu, J. S. Zhao, Y. X. Zhang, H. Zhou, X. Q. Li, X. H. Li, *Energy Environ. Sci.*, **2021**, *14*, 5406-5415.
- [34] Y. Cai, J. Cui, M. Chen, M. M. Zhang, Y. Han, F. Qian, H. Zhao, S. M. Yang, Z. Yang, H. T. Bian, T. Wang, K. P. Guo, M. L. Cai, S. Y. Dai, Z. K. Liu, S. Z. Liu, *Adv. Funct. Mater.*, **2021**, *31*, 2005776.
- [35] W. J. Zhao, J. Xu, K. He, Y. Cai, Y. Han, S. M. Yang, S. Zhan, D. P. Wang, Z. K. Liu, S. Z. Liu, *Nano-Micro Lett.*, **2021**, *13*, 169-172.
- [36] X. F. Ling, H. W. Zhu, W. D. Xu, C. Liu, L. F. Pan, D. Ren, J. Y. Yuan, B. W. Larson, C. Grätzel, A. R. Kirmani, O. Ouellette, A. Krishna, J. G. Sun, C. Y. Zhang, Y. Y. Li, S. M. Zakeeruddin, J. Gao, Y. H. Liu, J. R. Durrant, J. M. Luther, W. L. Ma, M. Grätzel, *Angew. Chem. Int. Ed.*, **2021**, *60*, 27299-27306.
- [37] Y. Wang, X. M. Liu, T. Y. Zhang, X. T. Wang, M. Kan, J. L. Shi, Y. X. Zhao, *Angew. Chem. Int. Ed.*, **2019**, *58*, 16691-16696.
- [38] X. T. Wang, Y. Wang, Y. T. Chen, X. M. Liu, Y. X. Zhao, *Adv. Mater.*, **2021**, *33*, 2103688.
- [39] S. B. Xiong, Y. Dai, J. M. Yang, W. Xiao, D. Q. Li, X. J. Liu, L. M. Ding, P. P. Cao, M. Fahlman, Q. Y. Bao, *Nano Energy*, **2021**, *79*, 105505.
- [40] S. M. Yang, W. D. Liu, Y. Han, Z. K. Liu, W. J. Zhao, C. Y. Duan, Y. H. Che, H. S. Gu, Y. B. Li, S. Z. Liu, *Adv. Energy Mater.*, **2020**, *10*, 2002882.
- [41] C. Y. Duan, J. Cui, M. M. Zhang, Y. Han, S. M. Yang, H. Zhao, H. T. Bian, J. X. Yao, K. Zhao, Z. K. Liu, S. Z. Liu, *Adv. Energy Mater.*, **2020**, *10*, 2000691.
- [42] X. Guo, B. Zhao, K. X. Xu, S. M. Yang, Z. K. Liu, Y. Han, J. Xu, D. F. Xu, Z. A. Tan, S. Z. Liu, *Small*, **2021**, *17*, 2102272.

COMMUNICATION

WILEY-VCH

Table of Contents



Herein, a new passivator---benzoyl hydrazine (BH) which has carboxyl, hydrazine and phenyl groups was developed to effectively passivate defects in CsPbI₃ through synergetic effects of these groups. Consequently, the highest efficiency of 20.47% with high open-circuit voltage and stability is achieved in a BH-CsPbI₃ solar cell, the highest efficiency among all pure CsPbI₃-based devices reported to date.

Yuhang Che,^[a] Zhike Liu,^{*[a]} Yuwei Duan,^{*[a]} Jungang Wang,^[a] Shaomin Yang,^[a] Dongfang Xu,^[a] Wanchun Xiang,^[a] Chao Wang,^[a] Ningyi Yuan,^[c] Jianning Ding,^[c] and Shengzhong (Frank) Liu^{*[a,b]}

Accepted Manuscript